Seismic behaviour of different types of masonry spandrels

A. Dazio[1]
EUCENTRE, Pavia, Italy

K. Beyer[1]
Ecole Polytechnique Fédérale de Lausanne (EPFL), Switzerland

ABSTRACT:
Most residential buildings that were constructed during the last century in Switzerland are 2-6 storey unreinforced masonry (URM) structures. At the beginning of the century, houses were constructed with timber floors and small bricks. This type of construction was later replaced by one which used larger, perforated bricks and reinforced concrete slabs. When assessing the seismic risk in Switzerland, a good understanding of the performance of the different types of URM buildings is mandatory. Numerical analyses have shown that spandrel beams have a significant influence on the seismic behaviour of URM structures since they influence strongly the stiffness and strength of the structure. However, until today, spandrel elements are often not considered when modelling URM structures because only very limited information on their force-deformation characteristics is available. For this reason a research project was initiated that aims at investigating the behaviour of different configurations of spandrel beams in URM walls using numerical and experimental methods. As part of the project full-scale, quasi-static monotonic and cyclic tests of spandrel beams were carried out. The test units represented spandrel beams in modern URM structures with reinforced concrete slabs or ring beams as well as spandrel beams in older URM structures with timber floors. This paper presents the results of the test campaign on masonry spandrels in URM structures with timber floors. Four spandrels were subjected to a quasi-static cyclic loading regime. The masonry spandrels were supported by either a timber lintel or a shallow masonry arch.

Keywords: Unreinforced masonry, spandrel, timber lintel, masonry arch, large-scale testing

1. INTRODUCTION

In unreinforced masonry (URM) structures vertical piers are connected by horizontal spandrel elements. Spandrels have been subjected to extensive damage during earthquakes and are often the first elements within a URM building to crack or fail. A typical failure mode of URM spandrels is shown in Fig. 1. It shows a building in L'Aquila after the M_w=6.3 earthquake on April 6th, 2009. All the spandrels between window openings have failed in shear and show the characteristic X-crack pattern. The horizontal stiffness and strength of the building are therefore very much reduced. In this particular building the spandrels are heavily restrained by both the relatively wide piers as well as by tension ties running along the facade embedded in the masonry. A different building is shown in Fig. 2, which was like the building in Fig. 1 closely located to the city centre of Aquila. In this case tension ties were not present. In addition the piers were very slender providing only a minor restraint to the axial elongation of the spandrels. As a consequence the spandrels failed in flexure by means of wide vertical cracks at both ends of the spandrel. Due to out-of-plane accelerations one of the spandrels collapsed completely. This building was a complete loss and was pulled down shortly after the earthquake.

[1] *Formerly at ETH Zürich, Switzerland*

Figure 1. Shear failure of spandrels with shallow masonry arches in an old URM building after the L'Aquila earthquake on April 6th, 2009: entire building (a) and detail of a spandrel (b).

Figure 2. Flexural failure of spandrels in an old URM building after the L'Aquila earthquake on April 6th, 2009: Entire building (a) and detail of a spandrel (b).

These two examples of URM buildings with spandrel elements show that, when analysing the global force-displacement characteristics of such URM walls, it is necessary to account for the coupling action of the horizontal spandrel elements. In the past, the effect of the spandrel elements was often neglected since experimental evidence of the force-displacement characteristics of the spandrel elements was missing. At present research efforts in Italy at the University of Trieste (Gattesco *et al.*, 2008) and at the University of Pavia (Grazziotti *et al.*, 2009) are underway to investigate experimentally the behaviour of URM and stone masonry spandrels, respectively. Within the research project carried out by the authors at the ETH Zürich several full-scale test units of different types of spandrels were tested under quasi-static loading (Beyer *et al.*, 2010). The experimental programme was divided into two parts. The test units of the first part represented spandrels in more modern URM buildings while in the second part spandrels of older URM buildings were tested. The major differences between the two parts of the test program concern (i) the presence or absence of a reinforced concrete (RC) beam in the first and second part, respectively, and (ii) the brick type. This paper summarises the experimental campaign on masonry spandrels in older buildings. These tests included masonry spandrel elements with either a timber lintel or a shallow masonry arch to bridge the opening. In the following, the test setup, the properties of the test units and selected test results are presented.

2. MASONRY SPANDREL TEST UNITS

Four masonry spandrel test units were tested. Each test unit consisted of two piers and the spandrel element, which were constructed with full bricks with dimensions of 250x120x60 mm. The thickness of the masonry wall was 38 cm, which corresponds to one and a half times the length of a brick and

included a 1 cm wide head joint. The bricks were laid in an English bond pattern on both faces of the wall. The span of the spandrel was 1.18 m and the height of the spandrel was approximately 1.26 m.

Two of the test units (TUA and TUB) had masonry spandrels supported on timber lintels while the other two consisted of spandrels with shallow masonry arches (TUC und TUD). The timber lintel consisted of four timber beams laid next to each other. Each beam was 158 cm long and had a rectangular cross section approximately 10 cm wide and 14 cm high. The URM arch featured a rise of 12 cm, which corresponds to about 1/10 of the span. A drawing of the test units and photos of the spandrel details are given in Table 1. The latter also summarises the axial stress applied to the piers and the properties of the steel ties that introduced an axial load into the spandrel. In TUA and TUC the axial load in the spandrel was provided by means of two horizontal D13 mm Stahlton rods. The rods were post-tensioned at the beginning of the test and the force in the rods was kept constant during the test by means of hollow core jacks connected to a load follower.

Table 1. Loading scheme, spandrel type and details of the axial load application for the four test units.

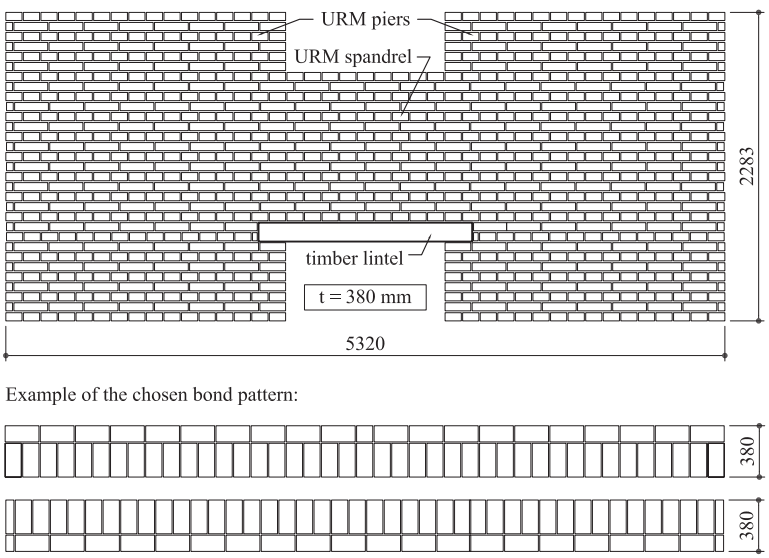

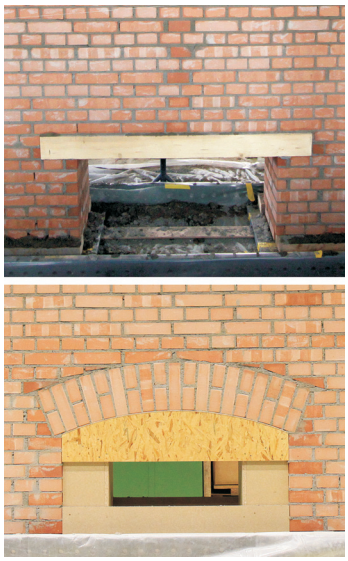

Test Unit	Loading	Spandrel type	Axial stress in piers	Steel tie
TUA	Cyclic	Timber lintel	0.33 MPa	Yes, prestressed to const. 40 kN
TUB	Cyclic	Timber lintel	0.33 MPa	Yes, plain bar, low axial stiffness
TUC	Cyclic	Masonry arch	0.43 MPa	Yes, prestressed to const. 80 kN
TUD	Cyclic	Masonry arch	0.43 MPa	Yes, plain bar, high axial stiffness

In real buildings the axial force in the spandrels will depend on the axial elongation of the spandrel and on the boundary conditions provided by adjacent piers and steel ties, if present. The axial force in the spandrel will therefore vary during seismic loading. While such a setup is surely more realistic for real buildings, a constant axial load is easier to consider in the framework of numerical simulations. To study the effect of a varying axial force on the force-deformation characteristics of the spandrel, the axial load in the spandrels of TUB and TUD was provided by means of rods that were slightly pre-tensioned at the beginning and then locked-in. Fixing the length of the rods implied an axial force increase upon axial elongation of the spandrel. In TUB the axial load was provided by means of two D10 mm threaded rods, in TUD two D32 mm rods were used.

The goal of the tests was to provide high quality experimental evidence as a valuable benchmark for the validation and calibration of numerical and analytical models for URM spandrels with timber

lintels and masonry arches. For this reason it is important to note that both the dimensions and the application of the axial load on the spandrel were not meant to represent the exact loading conditions in a spandrel but were rather chosen to allow the repetition of behaviour patterns observed during real earthquakes, like the ones described in Section 1, while applying clearly defined boundary conditions.

3. TEST SETUP FOR SPANDREL TESTS

Each test unit consisted of two piers and the spandrel element. In the test stand the test unit stood on two stiff beams ("lever beams") that were supported on hinges at the centre line of the piers and connected to servo-hydraulic actuators at their ends (Fig. 3). The support of the South lever beam allowed next to a rotation also a sliding movement along the longitudinal axis of the beam. Hence, the test stand did not restrain the axial elongation of the spandrel. To apply an axial load to the spandrel, two horizontal rods introduced an axial force into the spandrel, which was either constant throughout the test (TUA and TUC) or dependent on the axial elongation of the spandrel (TUB and TUD). The two piers were post-tensioned by four vertical rods each. The forces in the vertical rods were kept constant throughout the test. The purpose of these rods was to simulate the axial force in piers in real buildings. However, it should be noted that the piers in the test unit were not subjected to realistic moment and shear demands. The goal of the test campaign was not to test the piers but to test the spandrels. During testing the two actuators were moved with the same velocity in opposite directions. As a result the two horizontal lever beams rotated and the piers right and left of the spandrel were subjected to the same drifts, which caused the demand on the spandrel.

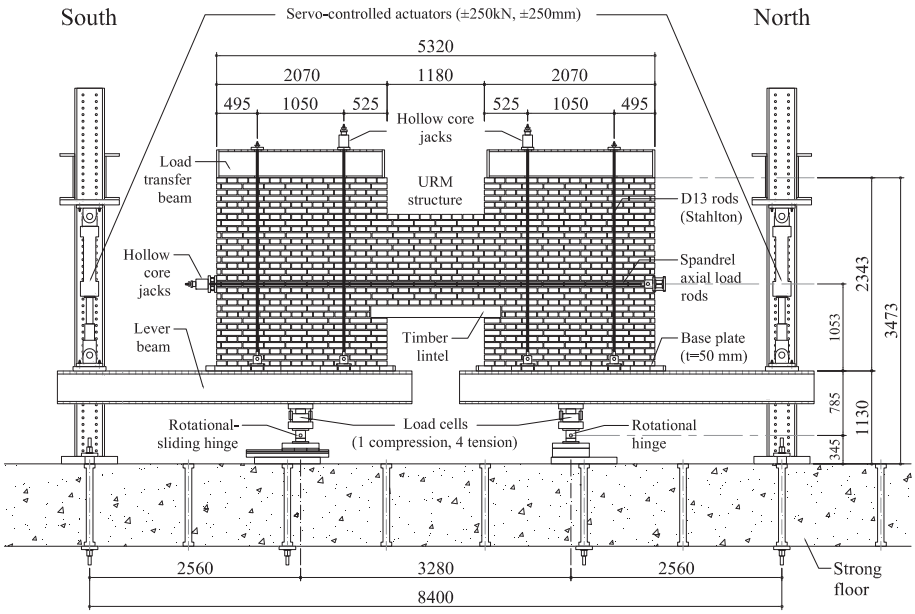

Figure 3. Drawing of the test setup for the masonry spandrel with timber lintel. View from the East without side restraint. All dimensions are in [mm].

4. INSTRUMENTATION AND LOADING HISTORY

Different global and local quantities were measured during testing by means of hard-wired instruments. These included (Fig. 4): (i) The actuator forces and the reaction forces at the supports of the lever beams, (ii) global deformation quantities, i.e. the rotation of the lever beams and the sliding movement of the South lever beam and (iii) the forces in the vertical and horizontal rods generating the axial load in the piers and spandrel, respectively. For TUA and TUB also the local deformation of the timber lintel was measured by means of linear variable differential transformer (LVDT) chains running along the top and bottom edges of the lintel's West face.

In addition to the hard-wired instruments, an optical measurement system (Optotrak Certus HD, NDI, 2009) was used to measure the local deformations of the test unit. The system works with a position sensor consisting of three cameras, which measured the 3D-coordinates of LEDs glued onto the test unit and base plates (see Fig. 6 and 7). The position of each LED defined through the time-histories of the x-, y- and z-coordinates was recorded with a rate of 10 Hz. During the post-processing the coordinate measurement data were first smoothed and then reduced to the same recording rate as the hard-wired data, i.e. to a frequency of 0.5 Hz.

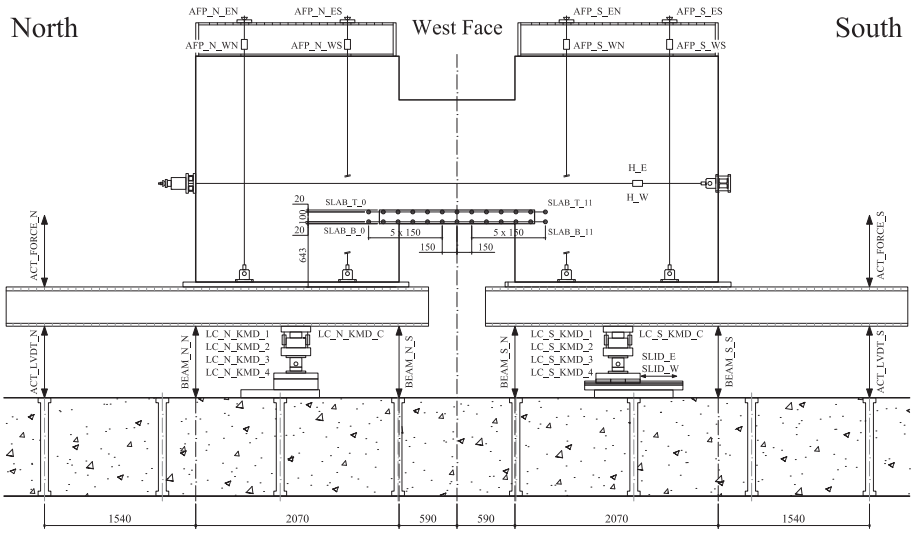

Figure 4. Layout of the hard-wired instruments for masonry spandrels with timber lintel. View from the West without side restraint. All dimensions are in [mm].

Quasi-static cyclic tests were performed and for each amplitude level two cycles were run. The considered amplitudes of the half-cycles corresponded to the following nominal drift levels θ_{nom}: 0.025%, 0.05%, 0.1%, 0.2%, 0.3%, 0.4%, 0.6%, 0.8%, 1.0%, 1.5%, 2.0%, 2.5%, 3.0%. A schematic figure of this loading scheme is shown in Fig. 5. A load step corresponds to a peak of one half-cycle of the loading history. The numbering of the drift-controlled load steps commences with LS 2. LS 0 refers to the state before any rotations or forces were applied. Afterwards, the axial load was applied to the piers (LS 1a) and the rods restraining the axial elongation of the spandrel were post-tensioned (LS 1b). At each load step the loading was stopped, cracks were marked and photos taken.

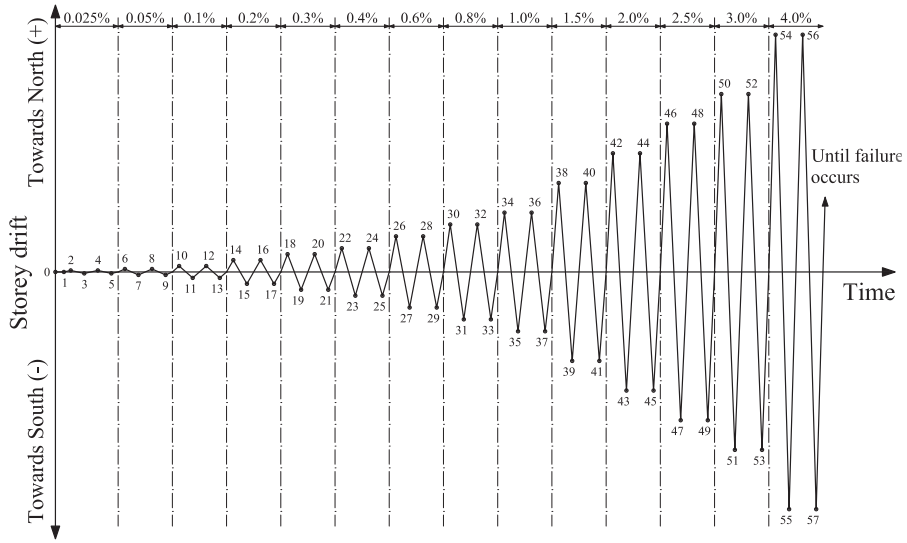

Figure 5. Loading history for quasi-static cyclic spandrel tests.

5. TEST RESULTS

The following discussion of the test results focuses on the failure mechanism and hysteretic behaviour of TUA and TUC. TUA had a timber lintel and TUC a masonry arch. Both test units were tested with a constant axial load applied to the spandrel. The axial load was, however, twice as large for TUC than for TUA (considering the cycles with pier rotations larger than 0.2%).

During the small cycles of TUA (up to a maximum pier rotation of 0.2%) the combination of axial load on the piers and axial load in the spandrel was modified two times. The test was started with an axial stress in the piers of 0.15 MPa and an axial force in the spandrel of 80 kN. It was then noted that part of the drift demand imposed by the rotation of the lever beams was absorbed within a base crack of the piers. This deformation was not intended. To eliminate this mechanism, the axial stress in the piers was increased to 0.33 MPa. However, even for this stress level, the crack at the base still opened up and therefore, as a second measure, the axial force in the spandrel was reduced to 40 kN, which corresponds to an average compression stress in the spandrel of about 0.08 MPa. In the following only the behaviour of TUA with this final configuration of axial loads is discussed (in Fig. 8a these cycles are plotted with a solid line).

Figure 6 shows the crack pattern for pier drifts of 0.4% and at failure for a drift of 3.0%. At θ_{nom}=±0.4%, for the positive direction of loading (Fig. 6a), the spandrel had developed a flexural mechanism with vertical cracks at both ends of the spandrel, which reached around the timber lintel. For the negative direction of loading (Fig. 6b), most of the deformations were absorbed by a large stair-stepped shear crack, which crossed the entire spandrel. As loading continued, such a diagonal crack developed also for the positive direction of loading. The final crack pattern of the spandrel corresponded to a mixed flexural-shear failure with vertical cracks at the end of the spandrel and shear cracks in the spandrel. The final failure of the test unit occurred for a drift of 3.0% and was associated with the failure of the supports of the timber lintel in the piers (Fig. 6c): They rotated inwards due to the horizontal shear stresses caused by the pull-out forces of the timber lintel.

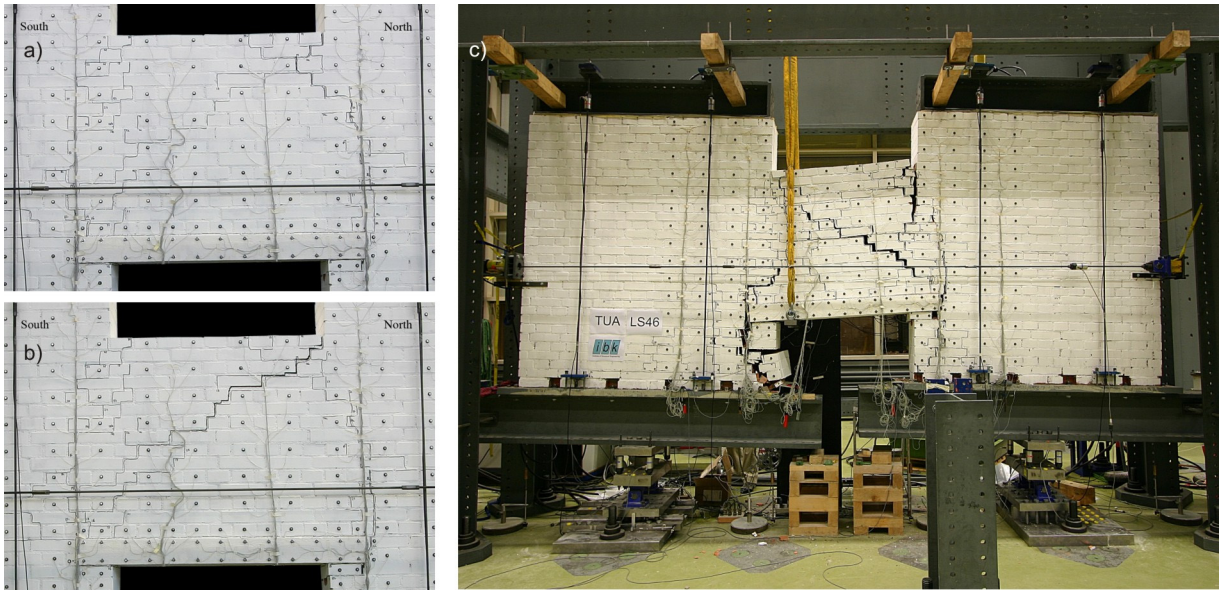

Figure 6. TUA: Crack pattern at LS 22 (θ_{nom}=+0.4%, a), LS 23 (θ_{nom}=-0.4%, b) and at LS 46 (failure of TUA at θ=+3.0%, c). Views from the East.

TUC featured a shallow masonry arch instead of the timber lintel. Similar to TUA the axial force in the spandrel was kept constant throughout the test but it was doubled to create a failure mode which was different to that of TUA. To reduce unrealistic deformations in the piers, the axial stress in the piers had been increased from 0.33 MPa to 0.43 MPa. TUC reached its peak shear capacity during the cycles with a rotation of 0.2%. During these cycles the spandrel failed in shear forming the

characteristic X-crack pattern, which has also been observed in real buildings (see Fig. 1). Figures 7a and 7b show the crack pattern of TUC for the positive and negative direction of loading, respectively, at a nominal drift of θ_{nom}=±0.4%. For both directions of loading the diagonal shear cracks were the widest cracks. Two hinges had formed in the arch, which were approximately located at 1/3 and 2/3 of the span. While the South hinge seemed to be mainly a flexural hinge, the North hinge showed already at θ_{nom}=±0.4% a significant sliding movement. This was most likely caused by the diagonal crack reaching into the spandrel from its South top corner. Unlike the other diagonal crack, it did not point to the corner of the spandrel but ended within this North plastic hinge of the arch. As loading continued the damaged to the arch increased with each cycle. The final failure occurred at a drift of θ=-3.5% due to collapse of the arch (Fig. 7c).

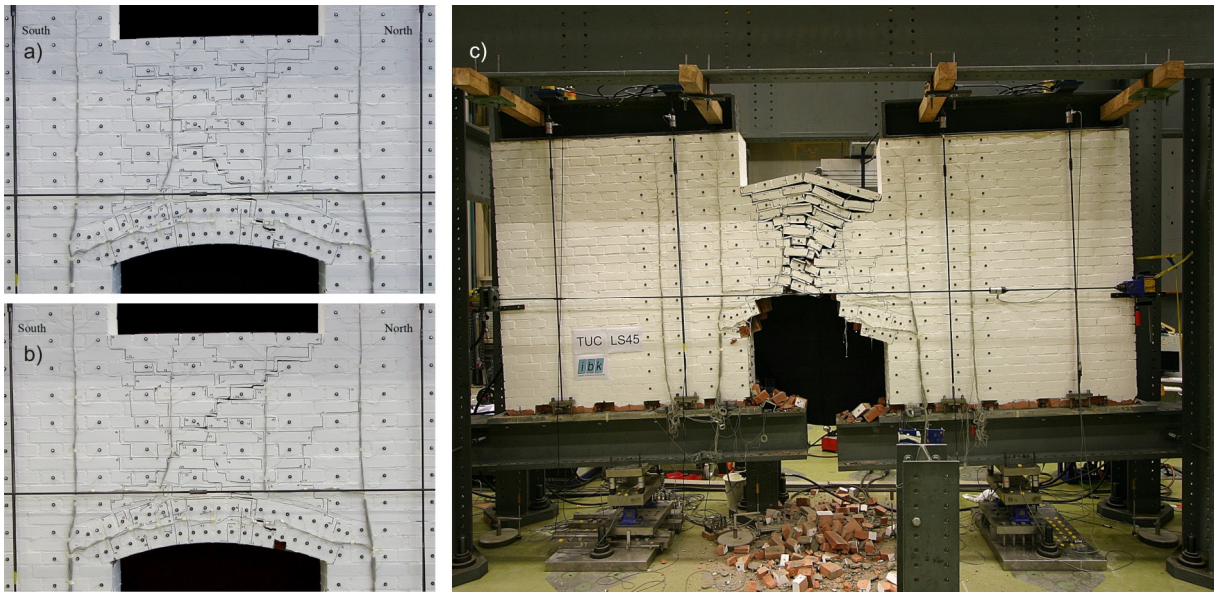

Figure 7. TUC: Crack pattern at LS 22 (θ_{nom}=+0.4%, a), LS 23 (θ_{nom}=-0.4%, b) and at LS 45 (failure of TUC at θ=-3.5%, c). Views from the East.

Figure 8 shows the force-rotation relationships for TUA and TUC. The average rotation is defined as the average rotation of the North and South lever beams and was computed from the LVDTs which were mounted underneath the lever beams (Fig. 4). The shear force in the spandrel was computed from the actuator forces, the reaction forces at the supports of the lever beams as well as the weight of the test units. For both tests, the maximum shear force was reached for a drift of about 0.2%. For TUA, the shear force dropped then relatively fast to a value of 65 kN, which remained nearly constant over a large portion of the test. This value is larger than the contribution provided by the axial force alone, which can be estimated as 42.7 kN (OPCM n. 3431, 2005). Hence, it appears that the lintel and the masonry spandrel were able to carry shear over a large deformation range.

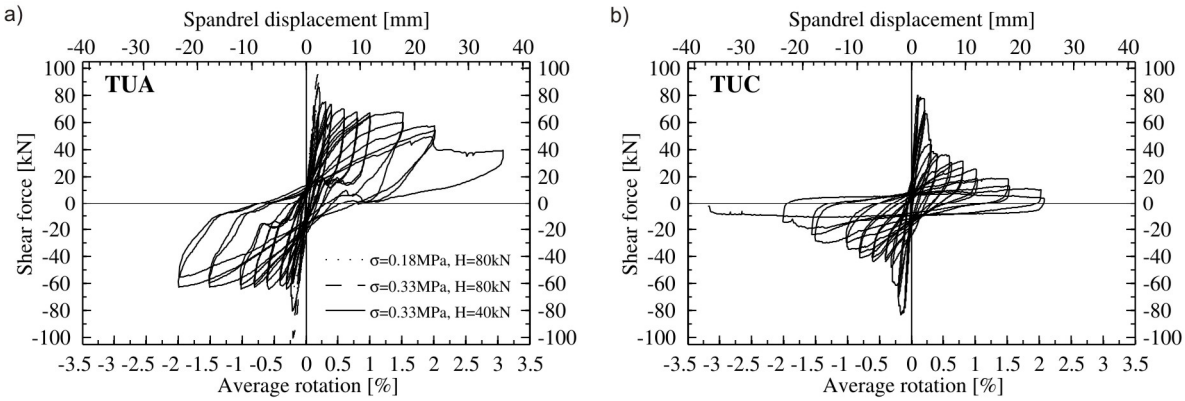

Figure 8. Force-rotation relationships for TUA (a) and TUC (b).

For TUC the reduction in shear force capacity after reaching the peak shear stress at θ_{nom}=+0.2% was larger than for TUA and continued until failure occurred, which was caused by the partial collapse of the arch. The drop in force was caused by the progressive crushing of the masonry arch, which led to a reduction in the static height of the spandrel. Even the peak shear force of TUC was smaller than the upper limit of the contribution of the axial force alone, which amounted to 85.4 kN (OPCM n. 3431, 2005). Like TUA, TUC failed at a drift demand, which was considerably larger than the ultimate state drift limits for piers, which are currently assumed as 0.4% and 0.8% drift for shear and flexural failure, respectively (CEN, 2005). The tests were continued beyond these limits. However, it is recommended to regard these results with caution when transferring them to real applications. This is for two reasons: (i) Possible damage to the piers during real earthquakes might modify the boundary conditions imposed on the spandrel while in the tests the piers remained over the entire range of rotation demand virtually undamaged. (ii) Out-of-plane accelerations might lead to out-of-plane failure of the masonry spandrels once the in-plane loading has disjointed the masonry spandrel (see Fig. 2).

6. CONCLUSIONS

The experiments presented in this paper provide high-quality data, which will allow the verification of numerical models of spandrel elements. At present, an in-depth analysis of the experimental data is underway, which should reveal additional insights into the load-bearing mechanisms of the different types of spandrels. In addition, numerical and mechanical modelling of the spandrels will be performed. The final objective of this research effort will be the development of new displacement-oriented guidelines for the design and assessment of buildings with composite and masonry spandrels.

ACKNOWLEDGEMENTS

Funding for this work was provided by the KGV Prevention Foundation in the framework of the research project "Nonlinear deformation behaviour of unreinforced masonry structures through testing and numerical simulations". The tests were carried out in the laboratory of the Institute of Structural Engineering at the ETH Zürich (Switzerland) where Dominik Werne, Thomas Jaggi and Christoph Gisler supported the authors during testing. All contributions are gratefully acknowledged.

REFERENCES

Beyer, K., Abo-El-Ezz A. and Dazio, A. (2010). Quasi-static cyclic tests on different types of masonry spandrels, *Tech. report*, Institute of Structural Engineering, ETH Zürich, Switzerland.

CEN. (2005). *Eurocode 8: Design of structures for earthquake resistance – Part 3: General rules, seismic actions and rules for buildings*. EN 1998-3. European Committee for Standardisation, Brussels, Belgium.

Gattesco, N., Clemente, I., Macorini, L. and Noè, S. (2008). Experimental investigation of the behaviour of spandrels in ancient masonry buildings, *Proc. of the 14th World Conference on Earthquake Engineering*, Beijing, China.

Graziotti F., Magenes G. and Penna A. (2009). Progetto di una sperimentazione su elementi di fascia muraria. *Rapporto Reluis, Allegato 4.3-UR01-1*, Università di Pavia e EUCENTRE, Pavia, Italy.

NDI (2009) *Optotrak Certus HD*, Northern Digital Inc., Waterloo, Ontario, Canada, http://www.ndigital.com/industrial/certushd.php, 2009.

OPCM n. 3431(2005). Ulteriori modifiche ed integrazioni all'OPCM n. 3274 del 20 marzo 2003, recante „Primi elementi in materia di criteri generali per la classificazione sismica del territorio nazionale e di normative tecniche per le costruzioni in zona sismica". *Suppl. Ordinario n. 85 alla G.U. n. 107 del 10 maggio 2005*. Ordinanza del Presidente del Consiglio dei Ministri del 3 maggio 2005. Rome, Italy.